Tellus
SERIES B
CHEMICAL
AND PHYSICAL
METEOROLOGY
PUBLISHED BY THE INTERNATIONAL METEOROLOGICAL INSTITUTE IN STOCKHOLM

Tellus (2009), 61B, 756–767

TELLUS

Aircraft study of aerosol vertical distributions over Beijing and their optical properties

By PENGFEI LIU[1], CHUNSHENG ZHAO[1]*, QIANG ZHANG[2], ZHAOZE DENG[1], MENGYU HUANG[1,2], XINCHENG MA[2] and XUEXI TIE[3], [1]*Department of Atmospheric Science, School of Physics, Peking University, Beijing, China;* [2]*Beijing Weather Modification Office, Beijing Meteorological Bureau, Beijing, China;* [3]*National Center for Atmospheric Research, Boulder, CO, USA*

(Manuscript received 7 December 2008; in final form 29 July 2009)

ABSTRACT

A set of 152 vertical profiles of aerosol number concentration and size distribution with diameter ranging from 0.12 to 3.0 μm observed by the airborne optical spectrometer probe in Beijing, China, between February 2005 and September 2006 is analysed and discussed. The statistic of aerosol number concentration (N_a) reveals a high aerosol number density in this region with average surface level number concentration (N_0) of about 6600 cm^{-3} (0.12–3.0 μm). The average vertical profile of N_a approximately satisfies an exponential decline function with a scale height of 1419 m. The N_a profiles are influenced by the structures of planetary boundary layer (PBL) significantly and two typical types of N_a profile under different conditions of PBL are presented and parametrized in this study. The observations of aerosol size distribution show that, in most cases the aerosol size distributions are not very sensitive to altitude, with effective radii ranging from 0.16 to 0.28 μm. Comparison between aircraft-derived aerosol optical depth (AOD) and Moderate Resolution Imaging Spectroradiometer-derived AOD shows good agreement. The Mie model calculations suggest that the surface level number concentration, the PBL height and the structure of PBL can influence the AOD significantly.

1. Introduction

Along with the rapid economic growth in China, an increasing anthropogenic emission of aerosol particles is having strong impacts on the regional air quality and the climate. In particular, aerosol particles influence the global radiation balance, which is a fundamental process that determines the climate by scattering and absorption of solar radiation (direct effect) (e.g. Charlson et al., 1992) and by serving as nuclei for formation of clouds (indirect effect) (e.g. Twomey, 1974; Albrecht, 1989). A recent study shows that the magnitude of precipitation in eastern central China has decreased significantly during the last 40 yr and the reduction of precipitation is strongly correlated to the high concentration of aerosol (Zhao et al., 2006). However, these effects induced by aerosols are difficult to be quantified (e.g. Haywood et al., 2003; IPCC, 2007). Especially, large uncertainties remain in the measurements of the aerosol vertical distributions in the low troposphere, which contains the bulk of aerosol mass (e.g. Gobbi et al., 2004). The aerosol vertical distribution has strong effects on the calculations of the direct and indirect radiative forcing (e.g. IPCC, 2007). There is a clearly need to better understand the aerosol vertical distribution.

Aerosol number concentration N_a (cm^{-3}) is usually considered as a crucial parameter in presenting the aerosol pollution conditions and an important factor for interacting with cloud formation. Aerosol effective radius R_e (μm) is another important parameter, which represents the mean size of the aerosol particles. The observed aerosol characterizations such as N_a and R_e are generally different within and above the planet boundary layer (PBL; see e.g., Spinhirne et al., 1979; Welton et al., 2002; Han et al., 2003). The structure of PBL is a key factor in determining the shape of the N_a vertical profiles inside the PBL. Above the PBL, the mineral dust from Gobi Desert could be lifted into the free troposphere (FT) and transported over thousands of kilometres to the eastern China (e.g. Zhang et al., 2006; Han et al., 2008), altering the vertical profile of size distribution and R_e significantly. Moreover, recent research indicates that aerosol pollutant near surface can be transported by local circulations, forming an elevated pollution layer in the FT with high concentration which is comparable to that within the PBL (Chen et al., 2009).

Such variable aerosol vertical distributions can alter the optical properties of aerosol such as aerosol optical depth (AOD) significantly, thus influencing the regional and global radiation

*Corresponding author.
e-mail: zcs@pku.edu.cn
DOI: 10.1111/j.1600-0889.2009.00440.x

balance. Therefore, more direct and long-term observations are needed to characterize the height-resolved aerosol properties and to provide essential validations for the models and the satellite remote sensing. Aircraft measurements are capable of providing high resolution in situ data of aerosol vertical distribution directly observed in the low troposphere (e.g. Bates et al., 1998; Collins et al., 2000a,b; Schmid et al., 2000; Anderson et al., 2003; Haywood et al., 2003; Zhang et al., 2006). However, because of the high operating costs, there is still a lack of aircraft measurements of the aerosol number concentrations and size distributions in the low troposphere over city areas of developing countries. As a mega city in China with population exceeding 15 million (National Bureau of Statistics of China, 2008), Beijing is suffering from severe air pollution problems driven by rapid development on both local and regional scales. To obtain the characterizations of aerosol and cloud in this region, intensive aircraft measurements were conducted during 2005 and 2006.

In this paper, we present a large number of aerosol vertical profiles (152) derived from 105 flights, which were carried out in Beijing region during the spring, summer and autumn in 2005 and 2006. After the introductions of the flight information, the aircraft instruments, the Moderate Resolution Imaging Spectroradiometer (MODIS) data and HYbrid Single-Particle Lagrangian Integrated Trajectory (HYSPLIT) model employed in the analysis and the method for data processing in Section 2, the vertical distributions of number concentration, effective radius and size distribution are analysed and discussed in Section 3. In Section 3.1, the average vertical profile and different types of vertical profiles of aerosol number concentration are presented, and a set of parametrized equations is developed to describe these profiles. In Section 3.2, different types of vertical distributions of effective radius and size distribution are illustrated and discussed. The optical properties of different aerosol vertical distributions are discussed in Section 4. In Section 4.1, Mie theory is applied to calculate the vertical profiles of aerosol extinction coefficient. Subsequently, the aircraft-derived AODs are estimated and compared with AOD derived from the satellite-borne MODIS instruments in Section 4.2. Section 4.3 designs eight scenarios of aerosol vertical distributions and the sensitivity of AOD to each factor of aerosol vertical distribution is estimated. A discussion and conclusion are presented in Section 5.

2. Methods and data

2.1. Flight information

Beijing is located in the north of Plain of North China. The urban area of Beijing is surrounded by mountains to the north, northwest and west. Tianjin and Shijiazhuang are another two big cities located in the Plain of North China to the southeast and southwest of Beijing, respectively. This study presents data from the flights in the Beijing region during the periods from February to October 2005 and from February to September 2006. The measurement was made by Weather Modification Office, Beijing Meteorological Bureau (WMOBMB) during the Beijing Urban Aerosol Measurement (BUAM) campaign. All measurements were carried out between 8:00 and 19:00 (local time).

Figure 1 shows the distribution of 2-yr (2005–2006) average of MODIS-derived AOD at 550 nm wavelength in Beijing region and the flight routes of all profiles we analysed for this study. The average MODIS AOD distribution is derived from NASA level 2 products. Two-year data of 2005 and 2006 were used to average at 0.1° × 0.1°grids. The MODIS AOD distribution shows a heavily polluted region from the southwest of Beijing region expanding to the south and west areas, with average AOD exceeding 0.6. The urban area of Beijing is polluted more heavily with average AOD exceeding 0.8. The north, northwest and west mountain areas are relatively clean. The flight areas are located

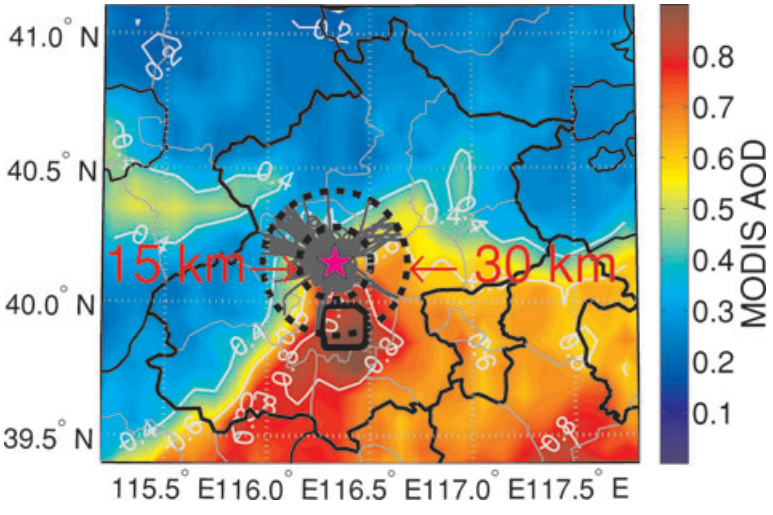

Fig. 1. Map of Beijing region shows location of study site (magenta pentacle), flight routes (grey lines), the 2-yr average MODIS AOD distribution (2005–2006, 0.1° × 0.1° resolution), and the urban area of Beijing city (the area in the thick solid black rectangle which represents the Fourth Ring Road of Beijing).

to the north of the urban area, near the northwest trim of the regional polluted area. Most of the vertical profiles are located in a circle with radius of 15 km, and all profiles are limited into a 30 km radius circle area. The average MODIS AOD value of the flight areas is about 0.6–0.8.

2.2. Instrumentation on the aircraft

Instruments employed in the observation were mounted on a multiengine aircraft (Cheyenne IIIA) to measure the size spectrum of particles, the meteorological parameters and the spatial locations simultaneously. The size spectrum of particles was measured by a particle measuring system (PMS Inc., Boulder, CO, USA), including a passive cavity aerosol spectrometer probe (PCASP) instrument and a forward scattering spectrometer probe (FSSP) instrument. Small and middle size particles with diameter ranging from 0.1 to 3.0 μm, such as sulphate, soot, organic carbon and smaller mineral dust particles were recorded by PCASP instrument with 15 unequally sized bins. The de-icing heater remained off during the whole field campaign. The FSSP instrument was applied to measure large (coarse) aerosol particles (e.g. larger mineral dust particles) and small cloud droplets with diameter ranging from 2 to 32 μm (Zhang et al., 2006). The meteorological parameters such as ambient air temperature (T) and dew point (Td) were also measured during flights and the relative humidity (RH) can be calculated subsequently. The real time locations such as longitude, latitude and altitude were recorded by a Global Positioning System (GPS) instrument. All instruments were operated at 1-s intervals. The speed of aircraft was about 100 m s^{-1} and the rate of climbing or descent of the aircraft was about 2–5 m s^{-1}. The particle measuring instruments (PCASP and FSSP) are calibrated using polystyrene latex spheres (PSL) by Particle Metrics Inc. (PMI) every year before the measurements take place. More detailed information regarding to the measurement instruments is provided by Zhang et al. (2006).

2.3. The MODIS data

The MODIS instruments mounted on Terra and Aqua satellites of NASA provide a global distribution of AOD, using multichannel information and pre-assumptions of aerosol type and size distribution. The MODIS aerosol products, which provide the AOD at 0.55 μm wavelength with spatial resolution of 10 km at nadir were released by NASA. These products were validated by Aerosol Robotic Network (AERONET) and the accuracy was estimated to be $\pm 0.05 \pm 0.2$ AOD (Chu et al., 2002;). In Beijing region, the MODIS AOD level 2 products were validated by handheld Sun photometers from Peking University and the result indicated that most of the data points were within the error range of 20% which was suggested by NASA (Chu et al., 2003; Li et al., 2003).

2.4. The HYSPLIT model

The HYSPLIT model is a complete system for computing simple air parcel trajectories to complex dispersion and deposition simulations, which was developed by NOAA and Australia's Bureau of Meteorology (Draxler and Rolph, 2003; Rolph, 2003). In order to identify the wind direction and the air mass origin of the long-range transport cases in our aircraft measurements, the newest internet based version of HYSPLT 4.9 was applied to calculate the 3-d backward-trajectories. In this study, the 3-hourly, $1^\circ \times 1^\circ$ spatial resolution NCEP's Global Data Assimilation Syste (GDASm) data archive was chosen as the gridded meteorological data which are necessary in the backward-trajectory calculations.

2.5. Theory and method

The number concentrations of particles with different diameters were recorded by PCASP or FSSP instruments, and each instrument has 15 size bins. The total number concentration $N_{\rm tot}$ (cm^{-3}) for each instrument is the sum of the concentration from all bins, which is expressed by

$$N_{\rm tot} = \Sigma_i N_i, \tag{1}$$

where $N_{\rm i}$ (cm^{-3}) is the particle number concentration at the ith bin. The effective radius $R_{\rm e}$ (μm) is calculated with the following equation:

$$R_{\rm e} = \Sigma_i N_i D_i^3 / \Sigma_i N_i D_i^2 / 2, \tag{2}$$

where $D_{\rm i}$ (μm) represents the geometry mean diameter at the ith bin, and $R_{\rm e}$ is the effective radius, which is a more useful parameter to represent the effective size of particles for aerosol optical properties. The aerosol normalized particle number size distribution (normalized PNSD) is defined as the following equation:

$$f(\log D_i) = N_i / \Delta \log D_i / \Sigma_i N_i = N_i / \Delta \log D_i / N_{\rm tot}, \tag{3}$$

where $\Delta \log D_i = \log D_i^{\rm upper} - \log D_i^{\rm lower}$, $D_i^{\rm upper}$ and $D_i^{\rm lower}$ refer to the upper and lower bounds at the ith bin, respectively. This function could demonstrate the vertical characteristic of aerosol number size distribution better than an unnormalized one, which is not divided by the total number concentration ($N_{\rm tot}$) of aerosol, for the reason that $N_{\rm tot}$ usually varies greatly as a function of altitude.

The FSSP instrument can measure both cloud droplets and coarse mode aerosol particles. The analysis of FSSP data combined with the manually recorded flight diary and the RH data show that, the FSSP number concentration $N_{\rm c}$ (cm^{-3}) measured in cloud generally ranges from 10 to several hundred cm^{-3} (Deng et al., 2009) and the RH is higher than 70%. By comparison, the FSSP number concentration measured in dust plumes is generally less than 10 cm^{-3}, and the RH is usually low. Only once in the heavy dust storm of 17 May 2006, coarse mode aerosol with FSSP number concentration values higher than 10 cm^{-3} (about

10–15 cm^{-3}) was observed in our study, with RH less than 20%. Here in this study we use the criteria that $N_c > 10$ cm^{-3} and RH > 70% to distinguish cloud areas from non-cloud areas.

In this paper, the aerosol number concentration N_a (cm^{-3}) refers to the total number concentration recorded by PCASP instrument. Due to the detection limit of the instrument, the data in the first bin (0.1–0.12 μm) is not accurate, and therefore they have been eliminated from the analysis. As a result, the characteristics of aerosol presented in this study represent that of aerosol with diameter ranging from 0.12 to 3 μm.

The Mie theory was applied to calculate the extinction profiles and the AOD, and to estimate the impacts of different aerosol vertical distributions on these optical properties. According to the Mie theory, the scattering cross-section σ_{sc} (μm^{-2}) and the absorption cross-section σ_{ab} (μm^{-2}) of a single spherical particle are determined by several important factors, including aerosol diameter D_p (μm), refractive index m and wavelength λ (μm). The extinction cross-section σ_{ex} (μm^{-2}) is the sum of σ_{sc} and σ_{ab}. Thus, the scattering coefficient k_{sc} (m^{-1}), absorption coefficient k_{ab} (m^{-1}) and total extinction coefficient k_{ex} (m^{-1}) are expressed as

$$k_{sc} = \Sigma_i \sigma_{sc} (\log D_i) n(\log D_i) \Delta \log D_i, \quad (4)$$

$$k_{ab} = \Sigma_i \sigma_{ab} (\log D_i) n(\log D_i) \Delta \log D_i, \quad (5)$$

$$k_{ex} = \Sigma_i \sigma_{ex} (\log D_i) n(\log D_i) \Delta \log D_i = k_{sc} + k_{ab}, \quad (6)$$

where $n(\log D_i)$ is the logarithms particle number concentration of the ith bin. The AOD can be calculated by integrating the extinction coefficient over height

$$\mathrm{AOD} = \int k_{ex}(h) dh. \quad (7)$$

2.6. Data selection and processing

Data applied in this study were carefully selected in order to accurately represent the characteristics of aerosol vertical distributions. An analysis procedure was applied to select aerosol vertical profile data.

(i) Exclude the data measured during hours with precipitation and the data observed in cloud areas. The precipitation hours were recorded in the flight diary, and the criteria to distinguish cloud conditions have been discussed in Section 2.5.

(ii) Select vertical profile data measured during aircraft ascending or descending to reveal characteristics of aerosol vertical distribution. According to our flight plan, the aircraft was spiraled down over the site to get vertical profiles before it landed. The diameters of the circles are about 10 km, and the upper bounds of these descending vertical profiles are generally 3600 m. To efficiently utilize the precious aircraft data, the ascending profiles with upper bounds higher than 1800 m (which is usually higher than the PBL heights) and horizontal distances less than 30 km from where the aircraft takeoff are also used in our analysis of vertical profiles.

(iii) Average data at 100-m height intervals and eliminate statistical outliers at the same time. We used the criteria that $|N_a - N_a^{avg}| > 3$ SD to find out statistical outliers at each specific altitude level, where N_a^{avg} is of mean value of N_a at a specific altitude level, and SD refers to the standard deviation.

As a result, we selected 152 vertical profiles from the original records of 105 flights with the procedure above, and the profiles selected were mostly undertaken in the spring, summer and autumn.

3. Experimental results

3.1. Vertical distributions of aerosol number concentration (N_a)

Vertical distributions of aerosol number concentration retrieved from aircraft measurements are presented in Fig. 2. It shows that the aerosol number concentration (N_a) near surface level ranges from 1000 to 10 000 cm^{-3} (10th to 90th percentiles), with an average value of 6600 cm^{-3}, indicating that the aerosol number concentration are generally very high in the Beijing region. The values of N_a generally decrease with altitude (grey lines in

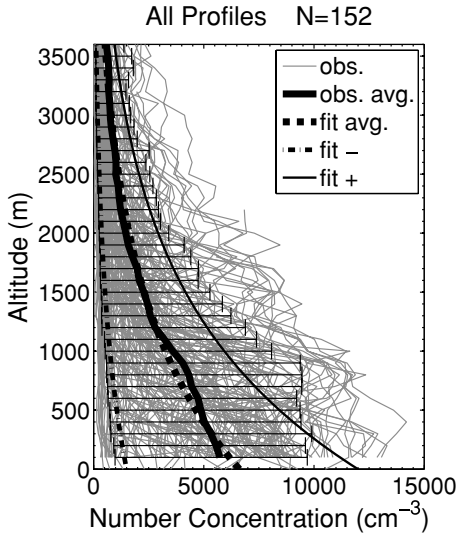

Fig. 2. All vertical profiles of aerosol number concentration (N_a). The solid black line, solid grey lines and horizontal error bars represent the average N_a vertical profile (obs. avg.), the observed N_a profiles (obs.) and the 10th and 90th percentiles of N_a values at each altitude level, respectively. The dashed black line shows a regression curve $N_a = 6612 \exp(-H/1419)$ [fit avg., see eq. (8) and Table 1] fitted to the average N_a vertical profile. The dash–dotted black line (left, fit–) and the thin solid black line (right, fit+) are assumed exponential decline curves representing the N_a profiles under the clean air condition and the heavily polluted condition, respectively. $N = 152$ represents that the number of profiles is 152.

Fig. 2). The average N_a profile (thick black solid line) appears to decrease with altitude exponentially, as shown in dotted black line in Fig. 2, which is expressed by the exponential equation as following:

$$N_a = N_0 \exp(-H/H_p), \tag{8}$$

where $N_0 = 6612$ cm^{-3} and $H_p = 1419$ m, representing the aerosol surface level number concentration and the aerosol scale height, respectively. These values are derived from the linear regression of the linear equation $\log N_a = -H/H_p + \log N_0$. The regression also suggests that $r^2 = 0.9881$ and rms $= 247$ cm^{-3}, where r is the correlation coefficient and root mean square (rms) represents root mean square errors of the fitted profile from the observed average profile. The black dash–dotted line (left-hand side) represents the vertical distributions under clean air condition (assume $N_0 = 1500$ cm^{-3}, $H_p = 1419$ m), while the thin solid black line (right-hand side) represents that of the heavily polluted condition (assume $N_0 = 12\,000$ cm^{-3}, $H_p = 1419$ m). This exponential decline profile of aerosol number concentration is consistent with the previous studies (e.g. Seinfeld and Pandis, 1997).

However, the vertical profiles of N_a vary greatly from case to case due to a variety of influences. The structure of PBL is a crucial factor, which determines the aerosol vertical distribution in the low troposphere. Two typical types of N_a vertical profiles are classified according to their different shapes, as shown in Fig. 3. Figure 3a1 shows the vertical profiles of N_a of the first type (defined as 'Na_type A'). The N_a values of this type profiles are generally uniform within the PBL, indicating that the aerosol pollutants are well mixed by the strong turbulence in the PBL but the concentration sharply decreases above the PBL. The PBL heights can be determined by the vertical profiles of N_a, and the results show that the PBL heights range from 500 to 1800 m with an average value of about 1000 m. Figure 3a2 shows the ambient temperature (T) profiles of Na_type A. This figure indicates that the T profile of Na_type A usually has elevated inversion layers at the top of PBL, which prevent the vertical diffusion of pollutant from the PBL to the FT. To better show the similarity of these profile shapes, the PBL heights of different profiles have been adjusted to the same level in these two figures; in Fig. 3a2 the temperatures of the top of PBL have been adjusted to the same value, too. In contrast, the vertical profiles of N_a and T of the second type (defined as Na_type B) are shown in Figs. 3b1 and b2, respectively. For Na_type B profiles, the values of N_a decrease rapidly with the increase of altitude. The T profiles of Na_type B show that the temperature gradients near surface are generally small, indicating that the surface layers are relatively stable and the turbulence is weak. The analysis of the flight dairy shows that the different situations of N_a profiles are basically related to the different weather conditions. In the Na_type A case, the sky is generally clear (57%) or partly cloudy (43%); most of the clouds are altocumulus or cirrus. In contrast, most of the

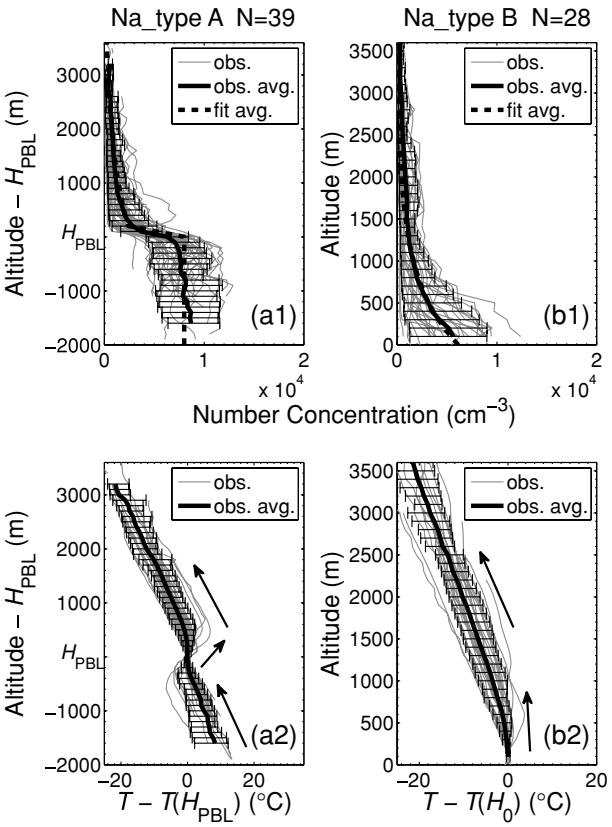

Fig. 3. Different shapes of aerosol number concentration (N_a) and temperature (T) profiles. (a1) and (a2) show the vertical profiles of N_a and T of Na_type A, representing cases with an elevated inversion layer at the top of PBL and a well mixed PBL below it; in these two figures the PBL heights of different profiles have been adjusted to the same level; in (a2) the temperatures at the top of PBL have been adjusted to the same value; (b1) and (b2) show the vertical profiles of N_a and T of Na_type B, representing cases with relatively stable surface layers. The dashed black lines show calculated profiles [fit avg., see eqs (8), (9) and Table 1] consistent with the average N_a vertical profile.

weathers of Na_type B are cloudy or overcast (82%); the clouds are usually stratocumulus, altocumulus or/and nimbus.

Different types of N_a vertical profiles discussed above can be empirically described by the following equations:

In the Na_type A case:

$$N_a = \begin{cases} N_0, \\ \qquad (\text{if } H < H_{PBL}); \\ N_0 - k \cdot (H - H_{PBL}), \\ \qquad (\text{if } H_{PBL} \le H < H_{PBL} + H_{LD}); \\ (N_0 - k \cdot H_{LD}) \exp\left(-\frac{H - H_{LD} - H_{PBL}}{H_p}\right), \\ \qquad (\text{if } H \ge H_{PBL} + H_{LD}). \end{cases} \tag{9}$$

where H (m), N_0 (cm^{-3}), H_{PBL} (m) represent the altitude, surface level number concentration and the height of PBL,

Table 1. Sets of values used in the empirical equations describing different types of N_a profiles

Na_Types	Equation no.	N_0[a] (cm^{-3})	H_p[b] (m)	H_{PBL}[c] (m)	H_{LD}[d] (m)	k[e] (cm^{-3} m^{-1})	RMS errors (cm^{-3})
Average	(8)	6612	1419	–	–	–	247
Na_type A	(9)	8000	1800	1000	200	28	438
Na_type B	(8)	6140	758	–	–	–	262

[a]Surface level aerosol number concentration.
[b]In eq. (8), H_p is the aerosol scale height; in eq. (9), H_p is the aerosol scale height in the free troposphere.
[c]The PBL height.
[d]The thickness of the linear decrease layer (LDL).
[e]The decreasing rate in LDL.

respectively; H_{LD} (m) is the thickness of a transition layer named linear decrease layer (LDL) where N_a decreases rapidly, and k (cm^{-3} m^{-1}) represents the decreasing rate in this layer; H_p (m) is the aerosol scale height above the LDL (in the FT).

In the Na_type B case, the vertical profiles generally decrease exponentially with altitude, and thus eq. (8) is applied to empirically describe this type of N_a profiles. However, the values of N_0 and H_p in eq. (8) applied for the Na_type B are different from those applied for the average profile (see Fig. 2), and the Na_type A applied another empirical equation (eq. 9) as mentioned above. In order to clearly describe different types of N_a profiles, several sets of value used for describing the N_a profiles of Na_type A, Na_type B and the average profile are given in Table 1. Comparisons between the calculated profiles and average profiles of the observation are illustrated in Fig. 3, the rms errors between them are also listed in Table 1. Compared with the N_a values, the rms errors are relatively small. These results indicate that the equations mentioned above could well describe the vertical structures of N_a profiles.

3.2. *Vertical distributions of aerosol effective radius (R_e) and particle number size distribution*

The effective radius (R_e) defined as the ratio of the third to the second moment of the aerosol number size distribution is an important parameter to describe the size and the optical properties of aerosol. Figure 4 depicts the vertical distributions of R_e of all profiles. It clearly indicates that most of the values of R_e are below 0.4 μm while profiles with the radius larger than 0.4 μm are sparsely distributed. The average R_e increases slightly with altitude. For the reason that R_e represents the mean size of aerosol, aerosol plumes with different R_e generally originated from different sources. Thus it is necessary to study different characteristics of aerosol vertical distributions by classifying aerosol profiles according to their effective radii.

In this study, two types of R_e profiles are classified and discussed. The profiles with maximum value of R_e smaller than 0.4 μm are classified as Re_type A, representing that the local or regional pollution is heavy and dominant and the effects of

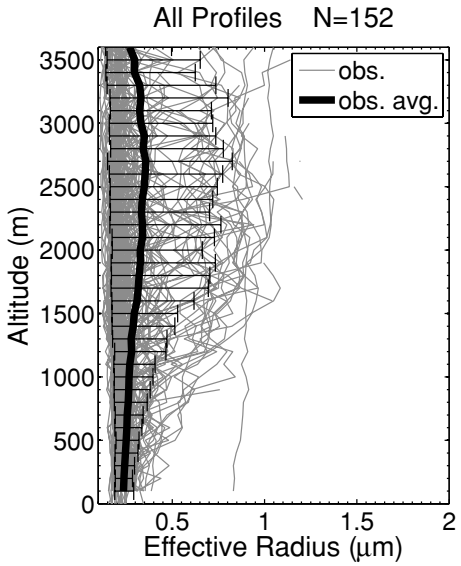

Fig. 4. Vertical distributions of the aerosol effective radius (R_e) of all profiles. Curves reported in the figure represent the average R_e vertical profile (black line, obs. avg), the observed R_e profiles (grey lines, obs.) and the 10th and 90th percentiles of data at each altitude level (the horizontal error bars).

long-range transport from desert areas are small. According to the flight dairy, RH data and the season, some profiles with larger R_e values are classified as Re_type B cases, representing that the effects of long-range transport of dusts from desert areas play an important role for the aerosol size distribution in the Beijing region. There are 102 profiles in Re_type A (67% of all profiles) and 27 profiles in Re_type B (18% of all profiles) in total. The other profiles (15% of all profiles) with R_e larger than 0.4 μm may be influenced by other processes such as clouds, high RH and smokes, while the detail analysis will be not presented in this paper.

Figure 5 illustrates the aerosol vertical distributions of R_e (see Figs. 5a1 and b1) and the average normalized PNSD (see Figs. 5a2 and b2) at different altitudes for Re_type A and Re_type B, respectively. As shown in Fig. 5a1, most R_e values

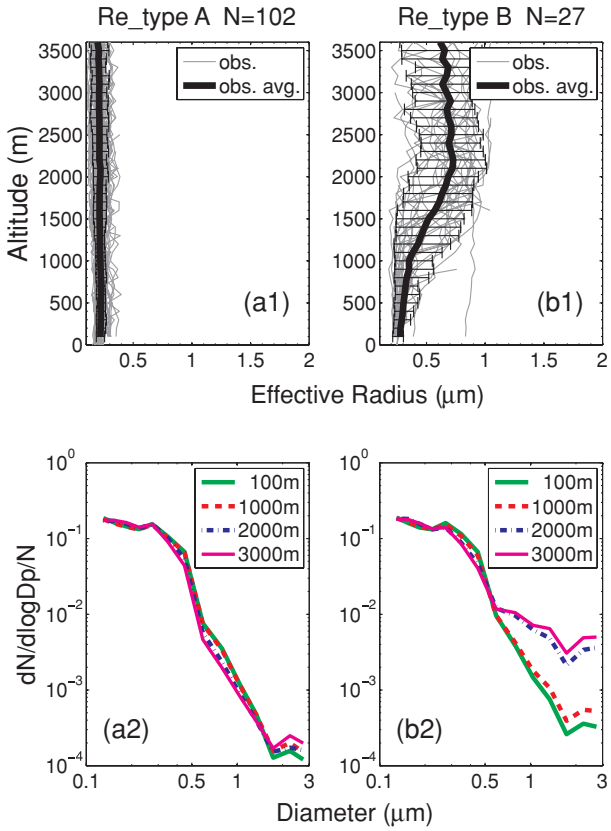

Fig. 5. (a1) and (b1): different types of R_e profiles; see Fig. 4 for the meanings of the curves; (a2) and (b2): average PNSD (normalized by the number concentrations) at 100, 1000, 2000 and 3000 m for different Re_type cases. Re_type A refers to the profiles dominated by the local/regional fine particle pollutions (with maximum R_e smaller than 0.4 μm); Re_type B refers to the profiles influenced by the long-range transport of dusts.

in the Re_type A case range from 0.16 to 0.28 μm, with an average value of about 0.22 μm, and the vertical variability is very small. In contrast, R_e vertical profiles in the Re_type B case show very different features compared to those in the Re_type_A case (see Fig. 5b1). For example, the average value of R_e near surface level is about 0.26 μm, which is comparable to the value of Re_type_A case. However, this value increases significantly at the height from 1000 to 2000 m. At the FT (above 2000 m) the values of R_e are very large (about 0.7 μm) and the variations with altitude are small, suggesting that these large aerosol particles outside the PBL come from a similar origin (mineral dust).

Accordingly, in Figs. 5a2 and b2, the differences in normalized PNSD between these two types are also presented. Figure 5a2 indicates that the shapes of the number size distributions of Re_type A at different altitude levels are very similar. This result also indicates that these aerosols at different altitudes are generally from the similar sources. Considering that Beijing is a heavily polluted mega city with a large population and other big cities such as Tianjin and Shijiazhuang are located nearby, the local or regional anthropogenic aerosol emissions could be the sources of the aerosol with vertical homogeneous shapes of number size distribution in Re_type A cases. By comparison, the normalized PNSD of Re_type B at different altitudes shown in Fig. 5b2 indicates that the shapes of number size distributions at different altitudes are very different, especially for the size greater than 0.5 μm. It is clear that the shapes of particle number distribution for the small particles (<0.5 μm) remain almost constant within and above the PBL while the proportion of large particles increases rapidly above the PBL height (2000 m) compared to the value within the PBL. By comparing the Figs. 5a2 and b2, we can also see that the shape of number size distribution of Re_type B near surface level is similar to the general shape of Re_type A. This indicates that a near-surface layer of aerosol from local (or regional) sources changes little even if the aerosol in higher altitudes changes a lot.

In order to confirm our assumption that the large-size particles observed in the Re_type B cases are related to the long range transport of mineral dusts, the wind directions and the air mass origins of the these cases are identified by the internet based HYSPLT model (Draxler and Rolph, 2003; Rolph, 2003). Figure 6 shows the 3-d backward-trajectories of all Re_type B cases at the surface level (100 m) and FT (2500 m). The transport paths indicate that the large-size particles observed by aircraft in Re_type B cases originated from the arid areas to the west of Beijing.

Figure 7 shows the time series of the mean values of R_e above 1500 m. Most of mean values of R_e above 1500 m are lower than 0.4 μm. In 2005, values of R_e larger than 0.4 μm were observed in April, May and the beginning of June. The peak of monthly average values is in April (see Fig. 7a). In 2006, the mean values of R_e above 1500 m larger than 0.4 μm occur in the springtime (March, April and May). These two figures indicate that the large-size particles in the FT occur more frequently in the springtime when the mineral dust events happen more frequently in the Beijing region (e.g. Kurosaki and Mikami, 2003; Zhao et al., 2004), suggesting that the vertical distributions of R_e and size distributions can be significantly affected by long-range transport of mineral dusts during the springtime in Beijing region.

4 The optical properties of aerosol vertical distributions

4.1. The extinction coefficient profiles derived from the aircraft measurements

The vertical profiles of aerosol number size distributions also provide useful information to better understand the aerosols optical properties. With the Mie theory, the extinction coefficient (k_{ex}) profiles and the AOD can be derived from the vertical

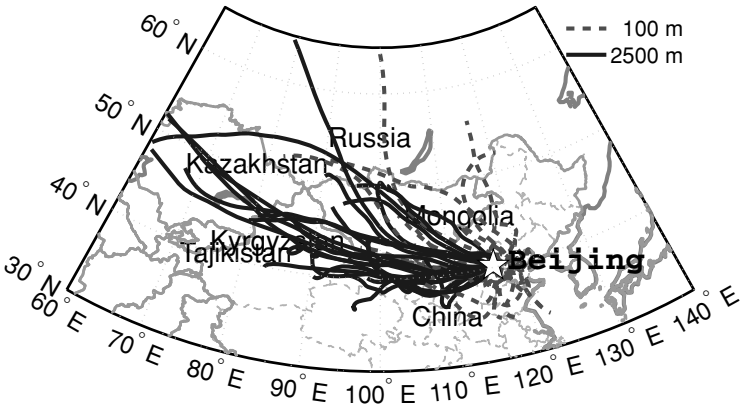

Fig. 6. Backward trajectories of the Re_type B cases at 100 m (surface level) and 2500 m (free troposphere) simulated by HYSPLIT model.

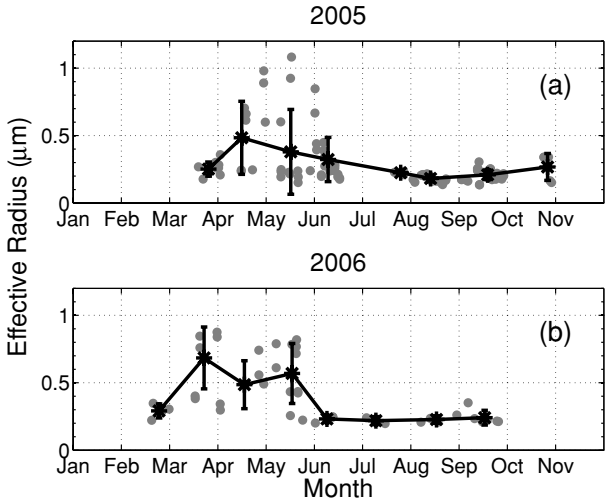

Fig. 7. Time series of mean R_e above the PBL in 2005 and 2006. The grey point represents the mean value of R_e above 1500 m of each profile; the black asterisks are monthly average values; and the error bars represent the standard deviation of data within 1 month.

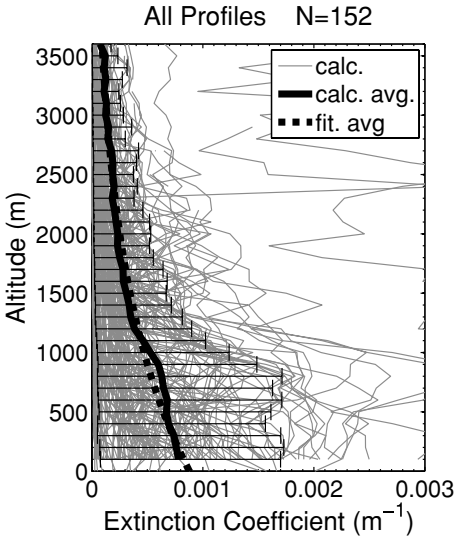

Fig. 8. The aerosol extinction coefficient (k_{ex}) profiles derived from the PNSD measured by PCASP. Curves reported in this plot represent the average k_{ex} vertical profile (black line, calc. avg), calculated k_{ex} profiles (grey lines, calc.), and the 10th and 90th percentiles of data at each altitude level (the horizontal error bars). The dashed black line (fit avg.) shows a regression curve $k_{ex} = 0.00088 \exp(-H/1601)$ fitted to the average k_{ex} vertical profile.

distributions of PNSD measured by aircraft. In the Mie scattering calculations, the refractive index m needs to be assumed. Considering that the PCASP instrument uses the manufacturer's recommended value $m = 1.585 + 0i$ to calculate the particle size (Strapp et al., 1992), this value is also used in the calculation from the PNSD to the extinction coefficient.

The calculated k_{ex} profiles are presented in Fig. 8. It shows that the k_{ex} profiles (grey lines) generally decrease with altitude, and the average k_{ex} profile (solid black line) decreases near exponentially. An exponential decline function (dashed black line in Fig. 8) is applied to depict the shape of average k_{ex} profile

$$k_{ex} = 0.00088 \exp\{-H/1601\}, \quad (10)$$

where H represents the altitude. The unit of k_{ex} is m^{-1} and the unit of H is m. The values applied in this equation are derived from the regression of the linear relation between log k_{ex} and H, with $r^2 = 0.9760$ and rms $= 4.88 \times 10^{-5}$ m^{-1}. This regression equation indicates that the average k_{ex} value at surface level is 0.00088 m^{-1} and the scale height of the average profile is about 1600 m. Both the curves in the figure and the rms value indicate that the errors of the regression equation are small from the average k_{ex} profile. This result can provide reference as an extinction profile over a heavily polluted mega city for the climate models.

4.2. *Comparison between the aircraft-derived AOD and the MODIS-derived AOD*

After the calculation of extinction profiles, the AOD was calculated by vertically integrating the extinction coefficients over the

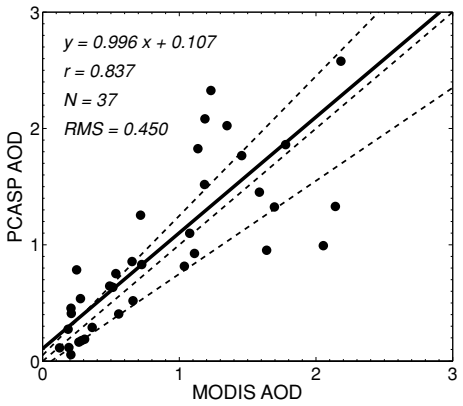

Fig. 9. The comparison between the aerosol optical depths (AOD) derived from the airborne PCASP size distributions (PCASP AOD) and the AOD derived from MODIS (MODIS AOD). The solid line represent the MODIS retrieval errors of $\Delta\text{AOD} = \pm 0.05 \pm 0.2$ AOD.

height. Profiles with maximum height higher than 2500 m were selected to conduct the comparison between the aircraft derived AOD and the MODIS AOD. Typically the maximum height of a profile is 3600 m, and the criteria we used to select profiles for the statistic of N_a, R_e and k_{ex} vertical distributions is 1800 m. For the reason that the aircraft-derived AOD is the layer AOD of the height range measured by the aircraft, while the MODIS AOD is the total AOD of the whole atmosphere, here a stricter criterion is applied to reduce the systematic error of integrating in the AOD calculation, ensuring that the selected profiles cover most of the extinction of the whole aerosol layer. The aircraft-derived AOD and the MODIS-derived AOD need to be colocated in both space and time, so that they could be compared with each other. To compare with aircraft-derived AOD, we calculated the average value of MODIS AOD data points obtained within 15 km in radius from the average location of each aircraft profile and at the same time within ±1.5 h from the average time of aircraft profile. The comparison results are shown in Fig. 9. The line of regression (solid black line) is $y = 0.996x + 0.107$, with 37 data points in total, correlation coefficient of 0.837 and rms of 0.45. The three dashed lines in the figure represent the 1:1 line (the middle one), $y = 0.05 + 1.2x$ (the upper one) and $y = -0.05 + 0.8x$ (the lower one). About 50% of the points are within the error range of MODIS estimated by NASA (Chu et al., 2003). Outside this range, the aircraft-derived AOD values of 5 points (14%) are lower than that derived from MODIS, whereas the values of 13 points (35%) are higher than that derived from MODIS. Considering that our flight areas are located at the joint between the polluted urban area and the relatively clean mountain area (as shown in Fig. 1), the spatial inhomogeneous of aerosol could partly response for the differences between the AOD derived from aircraft and MODIS. Temporal variation of aerosol distribution is another possible factor contributing to the differences. If stricter criteria of space and time applied for the colocation of aircraft-derived AOD and MODIS-derived AOD, the correlation coefficient would be higher and the rms would be lower, but the number of matched data points would be less, too. This comparison study indicates that the AOD derived from the airborne PCASP number size distribution is basically consistent with the MODIS AOD product. And it indirectly indicates that the calculation of extinction profiles is reasonable.

4.3. Impacts of the aerosol vertical distributions on the aerosol optical properties

From the previous discussions we can see that different factors, such as surface level number concentration (N_0), type of N_a profile (Na_type), type of R_e profile (Re_type) and the PBL height (H_{PBL}) can describe different aerosol vertical distributions and produce different extinction profiles and different AOD values. In the actual atmosphere, the extinction profiles and AOD are under the influence of various factors including those we already stated. In order to estimate the impact of each factor on the aerosol optical properties, eight scenarios of aerosol vertical distributions were designed and classified based on the previous analysis. The design scheme is described in Table 2. In S1, S2 and S3, we assumed that N_a decreases exponentially (see eq. 8) with the same scale height (H_p) of 1419 m (derived from average N_a profile) and with different surface level number concentrations (N_0) of 6612 cm^{-3} (average surface level number concentration),

Table 2. Surface level number concentration (N_0), types of Na profiles (Na_type), PBL height (H_{PBL}) and the types of R_e profiles (Re_type) set in the designed scenarios

Group	Case no.	N_0 (cm^{-3})	Na_type[a]	H_{PBL} (m)	Re_type[b]
Group 1	Case 1	6612	Average	–	Re_type A
	Case 2	12000	Average	–	Re_type A
	Case 3	1500	Average	–	Re_type A
Group 2	Case 1	6612	Average	–	Re_type A
	Case 4	6612	Na_type B	–	Re_type A
	Case 5	6612	Na_type A	1000	Re_type A
Group 3	Case 5	6612	Na_type A	1000	Re_type A
	Case 6	6612	Na_type A	1500	Re_type A
	Case 7	6612	Na_type A	500	Re_type A
Group 4	Case 1	6612	Average	–	Re_type A
	Case 8	6612	Average	–	Re_type B

[a]Na_type refers to the types of vertical profiles of aerosol number concentration (N_a); scenarios of Average, Na_type A and Na_type B employ the empirical equations (see eqs 8 and 9) with values assigned according to all observed profiles, the Na_type A profiles and the Na_type B profiles, respectively.

[b]Re_type refers to the types of vertical profiles of aerosol effective radius (R_e). Re_type A employ the average normalized PNSD derived from all observed Re_type A profiles, which is uniform with altitude; while Re_type B applies the height-resolved average normalized PNSD derived from the observed Re_type B profiles.

12 000 cm^{-3} (high surface level number concentration case) and 1500 cm^{-3} (low surface level number concentration case), respectively. In S4, we assumed that N_a decreases exponentially (see eq. 8) with the scale height (H_p) of 758 m (derived from the Na_type B case) and the surface level number concentrations (N_0) of 6612 cm^{-3} (average of all profiles). This scenario represents a typical case of Na_type B. Similarly, S5 assumed a same average level N_0 as S4, with different vertical distribution function of N_a (eq. 9), representing a typical case of Na_type A. S6 and S7 assumed same values for all parameters with S5, except for the height of PBL of 500 and 1500 m, representing low PBL case and high PBL case of Na_type A, respectively. In all of these scenarios except S8, a uniform size distribution derived from Re_type A profiles was applied, representing the dominant aerosol pollutants are from the local or regional sources. S8 applied a size distribution profile derived from Re_type B, with N_a of 6612 cm^{-3} and H_p of 1419 m, representing cases influenced by the long-range transport of dusts.

The groupings of these scenarios are also showed in Table 2. Group 1 scenarios (S1, S2 and S3) were designed to test the impact of surface level number concentration on the optical properties; group 2 scenarios (S1, S4 and S5) were chosen to show the impact of different shapes of N_a profile; group 3 scenarios (S5, S6 and S7) with different PBL heights under the well mixing PBL with elevated inversion layer condition were designed to estimate the impact of the PBL height; different vertical distributions of PNSD (associated to Re_type A and Re_type B, respectively) were applied in group 4 scenarios (S1 and S8), in order to assess their impact on the aerosol optical properties.

k_{ex}, as a function of altitude at the wavelength of 0.55 μm, was estimated by Mie scattering theory for the eight scenarios mentioned above, as shown in Fig. 10. The results indicate that, different vertical distributions of N_a and PNSD produce different vertical distributions of k_{ex}. Comparing group 1 scenarios (S1, S2 and S3) we can see that the surface level number concentration is a main factor dominates the aerosol extinction profile; group 2 and group 3 scenarios (S1, S4, S5, S6 and S7) indicate that different heights and structures of PBL can produce different extinction profiles even the aerosol properties at surface level are similar; group 4 scenarios (S1 and S8) show that the long-range transport of mineral dusts can alter the aerosol extinction profile significantly.

Subsequently, the AOD at 0.55 μm wavelength of the eight scenarios were calculated by vertically integrating the extinction coefficient profiles, as shown in Fig. 11a. The relative impact of each factor of N_0, Re_type, Na_type and H_{PBL} on the calculated AOD was also quantified. The results are shown in Fig. 11b. It can be seen that the AOD under clean (S3) and heavily polluted (S2) surface level pollution conditions can change greatly (±80%) compared with that of the average level scenario S1. The big difference between the scenario with highest AOD (S2) and that with lowest AOD (S3) is attributed to the difference of

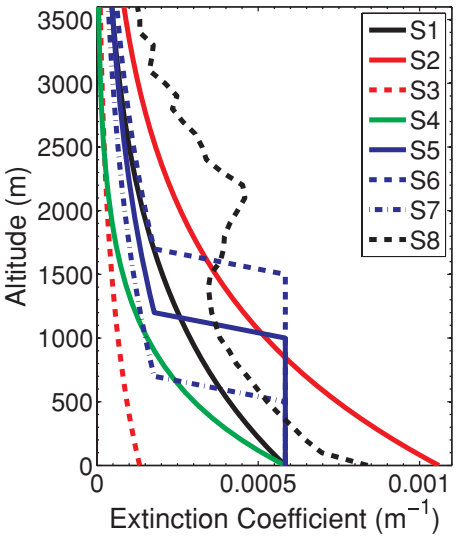

Fig. 10. Vertical profiles of extinction coefficient (k_{ex}) estimated by Mie theory for different scenarios designed in Table 2. See Table 2 for the descriptions of the scenarios.

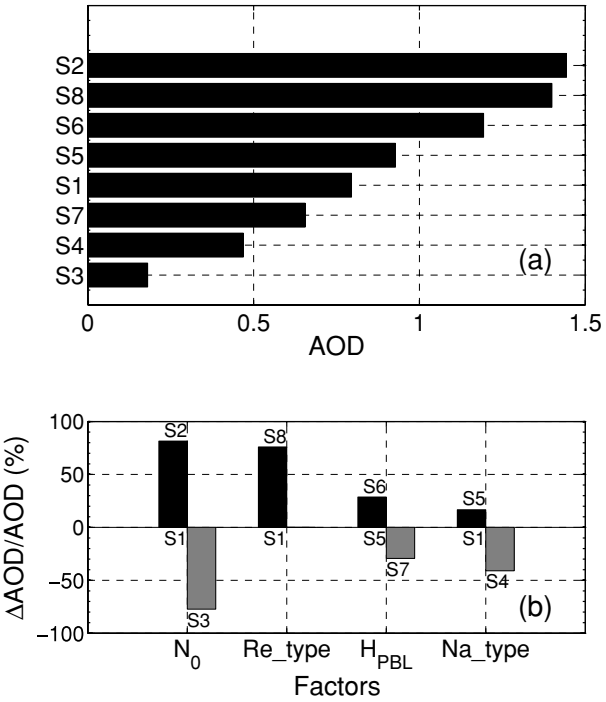

Fig. 11. (a) AOD (at 0.55 μm wavelength) of different scenarios defined in Table 2 estimated by Mie theory. (b) The relative impacts of different settings of types of surface number concentration (N_0), Re profiles (Re_type), PBL height (H_{PBL}) and types of N_a profiles (Na_type) on AOD calculations.

surface level number concentrations, suggesting that the local or regional generated fine particles play an important role in determining the AOD values. Compared with the local/regional aerosol dominant scenario (S1), the scenario of long-range

transport of mineral dusts can also produce significantly higher AOD (about +75%). The higher PBL height scenario (S6) also produces high AOD value (about 30% higher than the medium PBL height scenario S5), indicating that the PBL height is important in calculating the values of AOD. Different types of N_a profile (S4 and S5) determined by different PBL structures can also influence the AOD value significantly (−40% to +20%, compared to the average N_a profile scenario S1).

5. Conclusions

The measurements of vertical profiles of aerosol number concentration, effective radius and size distribution have been carried out using airborne PCASP instrument over the Beijing region. The overall characterization of aerosol vertical distributions has been presented using 152 vertical profile data derived from 105 flights.

Analysis of aerosol number concentration shows that the aerosol pollution is heavy in this region. The mean surface level number concentration in the diameter range of 0.12–3.0 μm is about 6600 cm^{-3}, and the mean vertical profile approximately satisfied an exponential decline function with a scale height of about 1419 m. Different N_a profiles were classified and presented, and the corresponding temperature profiles were also analysed to show the different structures of PBL. The structure of PBL is a crucial factor in determining the vertical distributions of number concentration. When the PBL is well mixed with an elevated inversion layer on the top, the aerosol number concentration is uniform within the PBL and declines rapidly above the inversion layer. This type of N_a profiles can be well described by a piecewise function. When the near-surface layer is relatively stable, the N_a decreases from the surface level with altitude increasing. An exponential decline function with scale height of 758 m is suggested to depict this type of N_a profiles.

The R_e profiles dominated by the local or regional pollution and those influenced by the long-range transport of mineral dusts were presented. In most of our observations, effective radii are not sensitive to altitude, and the values are small, within a narrow range between 0.16 and 0.28 μm, with mean value of about 0.22 μm. Their normalized PNSDs are similar at different altitudes, correspondingly. These cases were dominated by the local or regional anthropogenic aerosol pollutions. In contrast, several flights of our observations in the springtime suggested that the aerosol size distribution in the FT was significantly altered by the long-range transport of mineral dusts. Backward trajectory analysis suggests that the large-size particles were generally from the arid areas to the west of Beijing.

The extinction profiles and subsequently the AOD were estimated using Mie theory. An exponential decline equation with surface level extinction coefficient of 0.00088 m^{-1} and scale height of 1601 m was suggested to depict the average profile of extinction coefficient. The comparison study indicates that the calculated AOD derived from the airborne PCASP number size distribution are generally consistent with the satellite-borne MODIS AOD. The Impacts on aerosol optical properties of several factors, which relate to the aerosol vertical distributions were estimated and discussed. Eight scenarios were defined to quantify the sensitivity of each factor on the AOD calculation. The surface level number concentration was found to be a main factor which greatly alters the value of AOD (about ±80% compared to the average value); besides, the AOD values are also sensitive to the structure of PBL as well as the height of PBL (each factor could alter AOD about ±30%); when the PNSD influenced by the long-range transport of mineral dusts is applied in the calculation, the AOD value will significantly increase (about 75%) compared with that using the PNSD without influences of dusts.

6. Acknowledgments

This work is funded by the National Natural Science Foundation of China (NSFC) under Grant No. 40875001, Key Project of Natural Science Foundation of Beijing under Grant No. 80710002 and the National Key Technology R&D Program (2006BAC12B01). The authors are grateful to NASA/GSFC for the use of their MODIS Level 2 aerosol products. The authors also acknowledge the NOAA Air Resources Laboratory (ARL) for the provision of the HYSPLIT transport and dispersion model and READY website (http://www.arl.noaa.gov/ready.html) used in this publication.

References

Albrecht, B. A., 1989. Aerosols, cloud microphysics, and fractional cloudness. *Science* **245**(4923), 1227–1230.

Anderson, T. L., Masonis, S. J., Covert, D. S., Ahlquist, N. C., Howell, S. G. and co-authors. 2003. Variability of aerosol optical properties derived from in situ aircraft measurements during ACE-Asia. *J. Geophys. Res.* **108**(D23), 8647, doi:10.1029/2002JD003247.

Bates, T. S., Huebert, B. J., Gras, J. L., Griffiths, F. B. and Durkee, P. A. 1998. International Global Atmospheric Chemistry (IGAC) project's first aerosol characterization experiment (ACE-1): overview. *J. Geophys. Res.* **103**, 16297–16318.

Charlson, R. J., Schwartz, S. E., Hales, J. M., Cess, R. D., Coakley Jr., J. A. and co-authors. 1992. Climate forcing by anthropogenic aerosols. *Science* **255**(5043), 423–430.

Chen, Y., Zhao, C., Zhang, Q., Deng, Z., Huang, M. and co-authors. 2009. Aircraft study of mountain chimney effect of Beijing, China. *J. Geophys. Res.* **114**, D08306, doi:10.1029/2008JD010610.

Chu, D. A., Kaufman, Y. J., Ichoku, C., Remer, L. A., Tanre, D. and co-authors. 2002. Validation of MODIS aerosol optical depth retrieval over land. *Geophys. Res. Lett.* **29**(12), 1617–1621.

Chu, D. A., Kaufman, Y. J., Zibordi, G., Chern, J. D., Mao, J. T. and co-authors. 2003. Global monitoring of the air pollution over land from the Earth Observing System-Terra Moderate Resolution Imaging Spectroradiometer (MODIS). *J. Geophys. Res.* **108**(D21), 4661, doi:10.1029/2002JD003179.

Collins, D. R., Jonsson, H. H., Seinfeld, J. H., Flagan, R. C., Gasso, S. and co-authors. 2000a. In situ aerosol size-distributions and clear-column radiative closure during ACE-2. *Tellus* **52B**, 498–525.

Collins, D.R., Jonsson, H. H., Liao, H., Flagan, R. C., Seinfeld, J. H. and co-authors. 2000b. Airborne analysis of the Los Angeles aerosol. *Atmos. Environ.* **34**, 4155–4173.

Deng, Z., Zhao, C., Zhang, Q., Huang, M. and Ma, X. 2009. Statistical analysis of microphysical properties and the parameterization of effective radius of warm clouds in Beijing area. *Atmos. Res.* **93**, 888–896, doi:10.1016/j.atmosres.2009.04.011.

Draxler, R.R. and Rolph, G.D. 2003. HYSPLIT (HYbrid Single-Particle Lagrangian Integrated Trajectory) Model access via NOAA ARL READY Website (http://www.arl.noaa.gov/ready/hysplit4.html). NOAA Air Resources Laboratory, Silver Spring, MD.

Gobbi, G. P., Barnaba, F. and Ammannato, L. 2004. The vertical distribution of aerosols, Saharan dust and cirrus clouds in Rome (Italy) in the year 2001. *Atmos. Chem. Phys.* **4**, 351–359.

Han Y., Fang, X., Zhao, T. and Kang, S. 2008. Long range trans-Pacific transport and deposition of Asian dust aerosols. *J. Environ. Sci.* **20**, 424–428.

Han Z., Montague, D. C. and Snider, J. R. 2003. Airborne measurements of aerosol extinction in the lower and middle troposphere over Wyoming, USA. *Atmos. Environ.* **37**, 789–802.

Haywood, J., Francis, P., Dubovik, O., Glew, M. and Holben, B. 2003. Comparison of aerosol size distributions, radiative properties, and optical depths determined by aircraft observations and Sun photometers during SAFARI 2000. *J. Geophys. Res.* **108**(D13), 8471, doi:10.1029/2002JD002250.

IPCC. 2007. *Climate Change 2007: The Physical Science Basis*. Cambridge University Press, Cambridge, UK and New York, USA. 996.

Kurosaki, Y. and Mikami, M. 2003. Recent frequent dust events and their relation to surface wind in East Asia. *Geophys. Res. Lett.* **30**(14), 1736, doi:10.1029/2003GL017261.

Li, C., Mao, J., Lau, K. A., Chen, J., Yuan, Z. and co-authors. 2003. Characteristics of distribution and seasonal variation of aerosol optical depth in eastern China with MODIS products. *Chin. Sci. Bull.* **28**(22), 2488–2495.

National Bureau of Statistics of China. 2008. *China's Population and Employment Statistic Year Book 2008*. China Statistic Press, Beijing, China, 2–3.

Rolph, G.D. 2003. *Real-time Environmental Applications and Display sYstem (READY)* Website (http://www.arl.noaa.gov/ready/hysplit4.html). NOAA Air Resources Laboratory, Silver Spring, MD.

Schmid, B., Livingston, J. M., Russell, P. B., Durkee, P. A. and co-authors. 2000. Clear-sky closure studies of lower tropospheric aerosol and water vapor during ACE-2 using airborne sunphotometer, airborne in-situ, space-borne, and ground-based measurements. *Tellus* **52B**, 568–593.

Seinfeld, J. H. and Pandis, S. N. 1997. *Atmospheric Chemistry and Physics*. John Wiley & Sons, Inc., New York, USA, 444–445.

Spinhirne, J. D., Reagan, J. A. and Herman, B. M. 1979. Vertical distribution of aerosol extinction cross section and inference of aerosol imaginary index in the troposphere by lidar technique. *J. App. Meteorol.* **19**, 426–438.

Strapp, J. W., Leaitch, W. R. and Liu, P. S. K. 1992. Hydrated and dried aerosol-size-distribution measurements from the particle measuring system FSSP-300 probe and the deiced PCASP-100X probe. *J. Atmos. Oceanic Technol.* **9**, 548–555.

Twomey, S., 1974. Pollution and the planetary albedo. *Atmos. Environ.* **8**, 1251–1256.

Welton, E. J., Voss, K. J., Quinn, P. K., Flatau, P. J., Markowicz, K. and co-authors. 2002. Measurements of aerosol vertical profiles and optical properties during INDOEX 1999 using micropulse lidars. *J. Geophys. Res.* **107**, 8019, doi:10.1029/2000JD000038.

Zhang, Q., Zhao, C., Tie, X., Wei, Q., Huang, M. and co-authors. 2006. Characterizations of aerosols over the Beijing region: a case study of aircraft measurements. *Atmos. Environ.* **40**, 4513–4527.

Zhao, C., Dabu, X. and Li, Y. 2004. Relationship between climatic factors and dust storm frequency in Inner Mongolia of China. *Geophys. Res. Lett.* **31**, L01103, doi:10.1029/2003GL018351.

Zhao, C., Tie, X. and Lin, Y. 2006. A possible positive feedback of reduction of precipitation and increase in aerosols over eastern central China. *Geophys. Res. Lett.* **33**, L11814, doi:10.1029/2006GL025959.